Laser and Particle Beams (2003), *21*, 393–402. Printed in the USA.

DOI: 10.1017/S0263034603213173

Evolution of the Rayleigh–Taylor instability in the mixing zone between gases of different densities in a field of variable acceleration

S.G. ZAYTSEV,[1] V.V. KRIVETS,[1] I.M. MAZILIN,[1] S.N. TITOV,[1] E.I. CHEBOTAREVA,[1]
V.V. NIKISHIN,[2] V.F. TISHKIN,[2] S. BOUQUET,[3] AND J.-F. HAAS[3]

[1]Krzhizhanovsky Power Engineering Institute, Moscow, Russia
[2]Institute of Mathematical Modeling, Moscow, Russia
[3]Commissariat à I'Energie Atomique, Bruyères le Châtel, France

(RECEIVED 29 May 2002; ACCEPTED 4 April 2003)

Abstract

The interaction of the mixing zone between two gases of different densities with compression waves and shock waves has been investigated. The characteristics of the mixing zone in which the Rayleigh–Taylor instability is developing have been analyzed. The evolution of the mixing zone volume and mass during the accelerated motion has been defined. A qualitative distinction in the evolution of the mixing zone under the influence of a continuous deceleration resulting from the interaction with the reflected compression wave—shockless deceleration—is revealed as compared to deceleration that is accompanied by appearance of a shock wave moving through the mixing zone—shock-induced deceleration.

Keywords: Compression waves; Mixing zone; Shock waves; Variable acceleration

1. INTRODUCTION

The experimental studies of a hydrodynamic instability between two media of different densities at their accelerated motion have been successfully conducted for the case of incompressible media at moderate physical parameters (Kucherenko *et al*., 1991; Youngs, 1992; Schneider *et al*., 1998).

The basic goal of the present study was to define the quantitative characteristics of the given phenomenon developing in compressible media.

2. THE EXPERIMENTAL SETUP

The investigation was carried out in a vertical tube closed at both ends (Zaytsev *et al*., 1991). The sketch of the setup is given in Figure 1. Prior to the experiment, the tube was hermetically divided into two parts with a plate P. After evacuation of the tube its upper part B was filled with a combustible mixture (gas B, density ρ_b), the lower part was filled with gas A (density $\rho_a \gtrless \rho_b$). The pressure of gases A and B was precisely set at 0.5 bar. As a combustible mixture, we use the hydrogen–oxygen mixture ($0.45H_2 + 0.55O_2$).

After removing the plate P from the tube, a mixing zone K_0 forms and the combustion of gas B is initialized. The flame front F, descending in the tube, generates a compression wave C in gas B. As a result of interaction of C with the mixing zone K_0, the latter accelerates downward. The refracted compression wave, being reflected on the bottom plate of the tube, forms the reflected compression wave that moves towards the mixing zone. The interaction of the reflected compression wave and the mixing zone results in the deceleration of the latter.

The diagnostic of the process is carried out using Mach–Zehnder interferometry. The flow patterns in the tube and the density distribution in vicinity of K at the stages of accelerated and decelerated motion were defined.

3. FUNDAMENTAL REGIMES OF THE MIXING ZONES EVOLUTION

The flame front F acquires a meniscus form during its motion in the tube. A characteristic peculiarity of the motion of the meniscus-shaped flame front F is the formation of one-dimensional flow—a planar compression wave—ahead of F

Address correspondence and reprint requests to: S.G. Zaytsev, Krzhizhanovsky Power Engineering Institute, Leninsky pr. 19, Moscow 117927, Russia. E-mail: s.g.zaytsev@mtu-net.ru

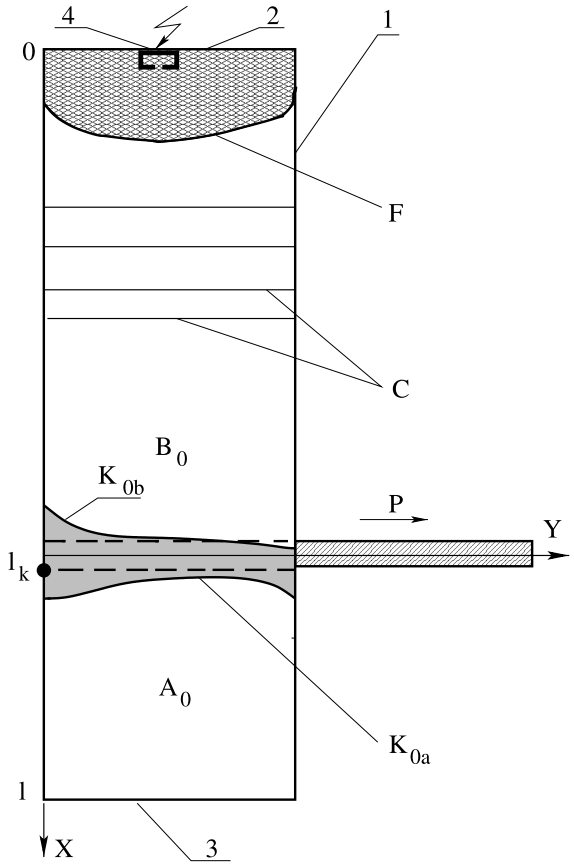

Fig. 1. The sketch of the experimental setup. 1: channel (inner section 72×72 mm^2, full length $l = 1010$–730 mm, length of the upper part $l_k = 63.5$ cm). 2, 3: upper and lower endwalls. 4: ignition spark. *P*: dividing plate. *F*: flame front, B_0: combustible mixture. A_0: inert gas. K_{0b}, K_{0a}: interfaces, separating the initial mixing zone from "pure" gases.

at a distance over a few diameters of a tube (Salamandra, 1974). The analysis of the motion shows that the essential changes of the flow parameters come from the dilatation of the combustion products behind F. This process determines the properties of the incident compression wave—C_0. The distribution of parameters within C_0 is modulated by a system of secondary compression waves.

The existence of secondary compression waves is clearly recorded in gases A, which have a large enough value of refraction coefficient (see Fig. 2). The density change in the front of secondary compression waves turns out to be smaller than in the incident compression wave—C_0. The secondary system of compression waves results from the interaction of the meniscus-shaped flame front with the lateral walls of the channel.

If the length of the upper part of the channel filled with the combustible mixture does not exceed a given threshold, then the compression wave C_0 during its motion does not succeed in turning into a shock wave. In that case, the initial mixing zone K_0 is involved in the accelerated motion by the compression wave. Hence, the following regimes of continuous acceleration of the mixing zone K are possible (see Fig. 3).

3.1. $\rho_a > \rho_b$

In this case, the direction of gravitational acceleration coincides with the direction of the density gradient and the mixing zone K_0 stays hydrodynamically stable until the beginning of the interaction with the compression wave C_0 ($t = t_0$). For $t \geq t_0$ the mixing zone K is accelerated down the channel by the incident compression wave. Here an effective gravitational field directed upward appears. The value of the acceleration of this field is $|g_1| \simeq 10^4 g_0$, where g_0 is the acceleration of the Earth's gravity. The Rayleigh–Taylor instability, (RTI), is excited in the mixing zone K ($\nabla\rho \cdot \nabla p < 0$).

The RTI development continues until the moment $t = t_Q$, when K deceleration, created by the interaction with the reflected compression wave C_R, begins. For $t \geq t_Q$ RTI "is switched off" as the effective gravitational field turns in the downward direction ($\nabla\rho \cdot \nabla p < 0$). The value of this acceleration field is $|g_2| \simeq 10^4 g_0$. At this stage of the mixing zone evolution, a "stratification" process "is switched on"—separation in the field of effective gravitation.

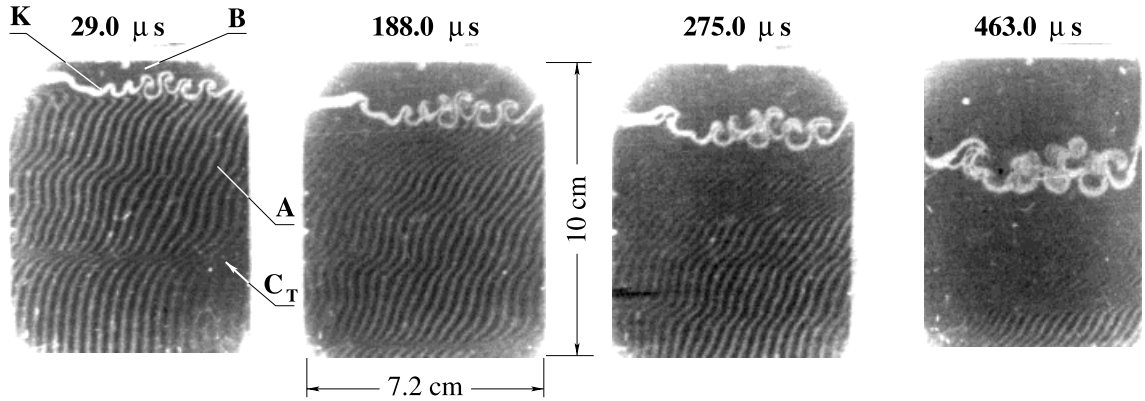

Fig. 2. Interferograms of the mixing zone motion, *K*, separating the combustible mixture from SF_6 ($p_0 = 0.5$ bar, $g \approx 1.3$ cm·s^{-2}). C_T: front of the first from the set of refracted compression waves.

https://doi.org/10.1017/S0263034603213173 Published online by Cambridge University Press

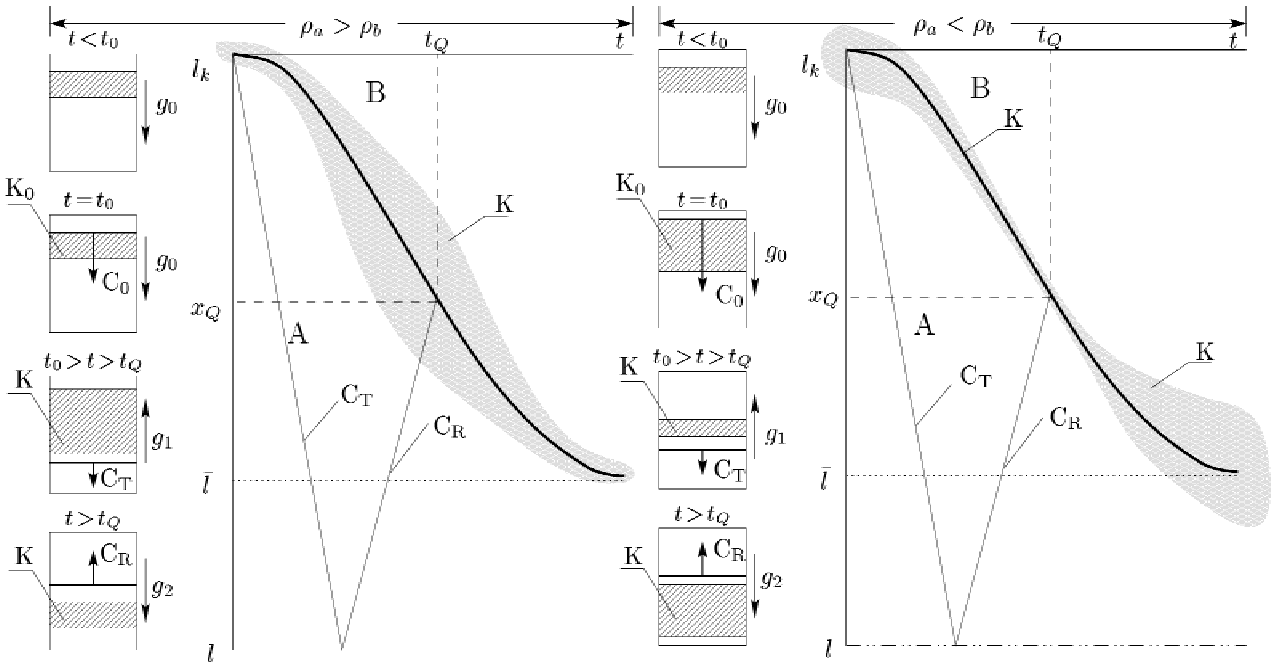

Fig. 3. Possible regimes of interaction between the mixing zone K and refracted C_T and reflected C_R compression waves.

At $t = \bar{t}$, the mixing zone K reaches the section $l = \bar{l}$, located at the minimum distance from the lower end of the channel. Later the mixing zone oscillates near $\bar{l}$ under the action of reverberating compression or rarefaction waves.

3.2. $\rho_a < \rho_b$

The change of the density gradient direction results in excitation of the hydrodynamic instability in the mixing zone K_0 in the Earth's gravitational field (acceleration g_0). This state continues until the compression wave arrival. In the stage of accelerated motion at $t_0 < t < t_Q$, K is subjected to an effective field ($|g_2| \simeq 10^4 g_0$), in the upward direction. Here the RTI "is switched off" ($\nabla\rho \cdot \nabla p < 0$). K is subjected to a compression, created by C_0.

In the deceleration stage created by the interaction of K with C_R at $t_Q < t < \bar{t}$, the RTI is excited and developed, as $\nabla\rho \cdot \nabla p < 0$.

Having reached the closest proximity from the lower channel plate (section $\bar{l}$) K oscillates under the action of reverberating waves in the compressed gas A.

4. THE INITIAL MIXING ZONE: MEASURED PARAMETERS

The plate P is removed from the channel with the help of a spring mechanism. The full time of removal of P from the channel ranges from 40 to 100 ms. The thickness of K_0 is determined by a diffusion coefficient of the gases A and B and by the time of mixing. The resulting mixing zone has the form of a layer that becomes thinner in the direction of the plate motion. The undulating perturbances on borders of the layer occur when the Reynolds number ($\mathrm{Re} = udv^{-1}$, where u is a flow velocity, d is a thickness of plate P, and v is a viscosity of gas A) exceeds 100. In Figure 4, a schematic representation of the mixing zone is given and the characteristic points J_i, B_j are indicated on the surfaces separating the mixing zone K_0 from gases B and A. The coordinates of the indicated points are used for definition of the following parameters of the mixing zone: amplitude a_i maximum penetration depth of one gas into the other L_i wave lengths of the chosen perturbation λ_i, trajectory of the mixing zone motion $x_k(t)$, thickness of mixing zone δ_i:

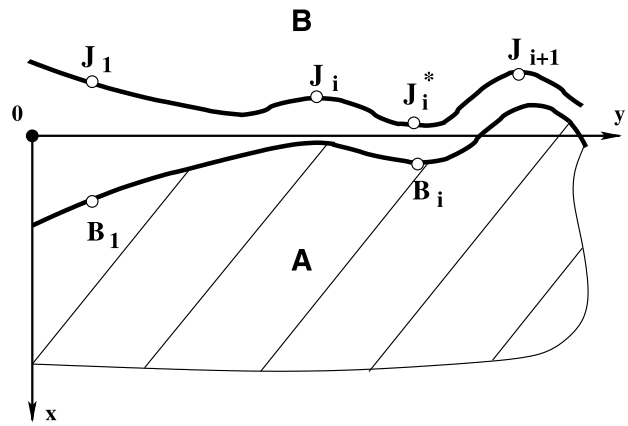

Fig. 4. A scheme of the initial mixing zone. J_i, J_i^*, J_{i+1}, B_i: position of characteristic points.

https://doi.org/10.1017/S0263034603213173 Published online by Cambridge University Press

$$\lambda_i = y(J_{i+1}) - y(J_i), \tag{1}$$

$$x_k(t) = x(B_i)/2 + [x(J_{i+1}) + x(J_i)]/4, \tag{2}$$

$$a_i = x(J_i^*) - [x(J_i) + x(J_{i+1})]/2, \tag{3}$$

$$L_i = x(B_i) - [x(J_i) + x(J_{i+1})]/2, \tag{4}$$

$$\delta_i = x(B_i) - x(J_i^*). \tag{5}$$

The value λ_i for the initial mixing zone decreases roughly by a factor of 2 along the direction of the plate motion (y axis). Near the channel axis ($y = 36$ mm), the quantity λ_i has the following values: 20, 18, 15, 12, 9, and 6 mm ± 2 for He, Ne, Ar, Kr, Xe, and SF_6, respectively, when the full time of the plate P removal equals 100 ms.

5. ONE-DIMENSIONAL MODEL

A flame front simulation is carried out using the subsequent heat release in the domain filled with the combustible mixture (gas B). In this domain, each cell of the computational mesh contains a source that releases a distributed quantity of energy $q(x)$. This energy is released in a precise time evolution such that the temperature in a given cell reaches the level of ignition temperature T_i. The temperature change in gas B comes as a result of the temperature wave propagation resulting from the energy release in the cells where combustion took place.

The flow in the channel closed at two ends is described by the system of conservation equation for mass, momentum, and energy in Lagrangian form:

$$\frac{d}{dt}(\rho\Delta) = 0, \tag{6}$$

$$\frac{d}{dt}u = -\frac{1}{\rho}\frac{\partial p}{\partial x} + \frac{\eta}{\rho}\frac{\partial^2 u}{\partial x^2}, \tag{7}$$

$$\frac{d}{dt}\varepsilon = -\frac{p}{\rho}\frac{\partial u}{\partial x} + \frac{\eta}{\rho}\left(\frac{\partial u}{\partial x}\right)^2 - \frac{1}{\rho}\frac{\partial}{\partial x}\left(\lambda\frac{\partial T}{\partial x}\right) + \frac{\partial q}{\partial t}. \tag{8}$$

This system is completed by the equation of state in the form

$$\varepsilon = \frac{p}{\rho(\gamma - 1)}. \tag{9}$$

Here ρ, ϵ, u, and λ are a density, internal energy, velocity, and thermal conductivity, respectively, Δ is the size of a cell of the Lagrangian mesh, $\eta \sim \rho\Delta$ is the factor of artificial viscosity. The variable x represents a Euler coordinate. As a respective Lagrangian coordinate, the so-called mass variable s, $ds = \rho dx$, was used. Thus equation (6) expresses both the condition of conservation of mass, and natural conditions of a constant of Lagrangian coordinate $ds/dt = 0$. For the solution of this equation system, the explicit numerical scheme (first-order time accuracy and second-order coordinate accuracy) was applied. The equation system was numerically solved with the following conditions: at the top $x = 0$ and bottom $x = l$ ends of the channel, the flow velocity is $u(t) = 0$. The combustible mixture (gas B) is set in the sector $0 \le x \le x_k - \delta/2$. Here, for x_k—the position of the median line of the mixing zone—at $t = 0$, $x_k = l_k$. The molar mass of the combustible mixture is $\mu_b = 18.5$. The specific thermal capacity ratio is $\gamma_b = 7/5$, where δ is the mixing zone thickness. One of the experimental gases A fills the sector $x_k + \delta/2 < x < l$, for which $\mu = \mu_a$, $\gamma = \gamma_a$, $q = 0$. The mixing zone is set in the interval $x_k - \delta/2 < x < x_k + \delta/2$, within which the density ρ varies according to a linear law from the density value ρ_b of gas B at the point $x_k - \delta/2$ to the value of density ρ_a of gas A at the point $x_k + \delta/2$. The flow in $0 < x < l$ is adiabatic.

Initial conditions are: the pressure of gas B, p_b, and the pressure of gas A, p_a, at $t = 0$ are equal to $p_b = p_a = p_0$. The ignition energy is $q = q_0$ at $t = 0$ for $x = 0$.

The shape of function $q(x)$ is determined from the agreement of calculated and experimentally measured position of trajectory of the mixing zone K at the initial stage of motion $t < t_Q$.

In Figure 5, the calculated density distribution $\rho(t)$ at the abscissa $x = 685$ mm is shown. The points in this picture are the experimentally measured values (Zaytsev *et al.*, 1999).

6. TWO-DIMENSIONAL MODEL

To calculate the evolution of the RTI, the solution of two-dimensional conservation equations is carried out with a nonlinear quasi-monotonic scheme of high precision (Nikishin *et al.*, 1994). The problem is investigated in a rectangular domain 7.2×100 cm^2, filled with gases A and B, which are separated by the mixing zone. The latter is accelerated by the compression wave propagating from B to A. The upper boundary of the calculated domain is set above

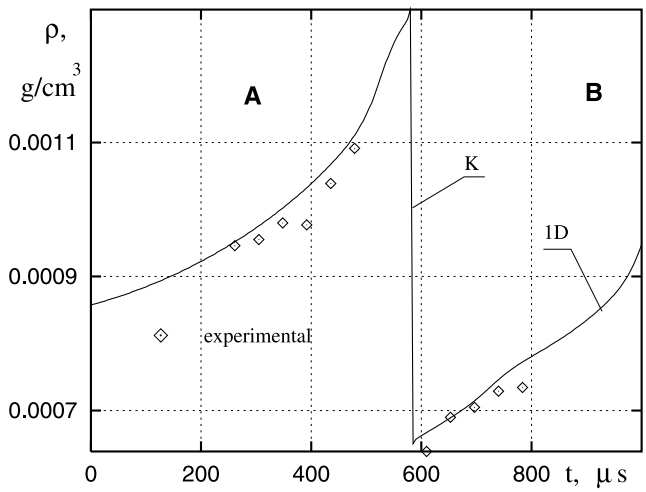

Fig. 5. Calculated (one-dimensional model) and experimental values of density $\rho(t, x_1)$, $x_1 = 68.5$ cm. K separates the combustible mixture from argon.

https://doi.org/10.1017/S0263034603213173 Published online by Cambridge University Press

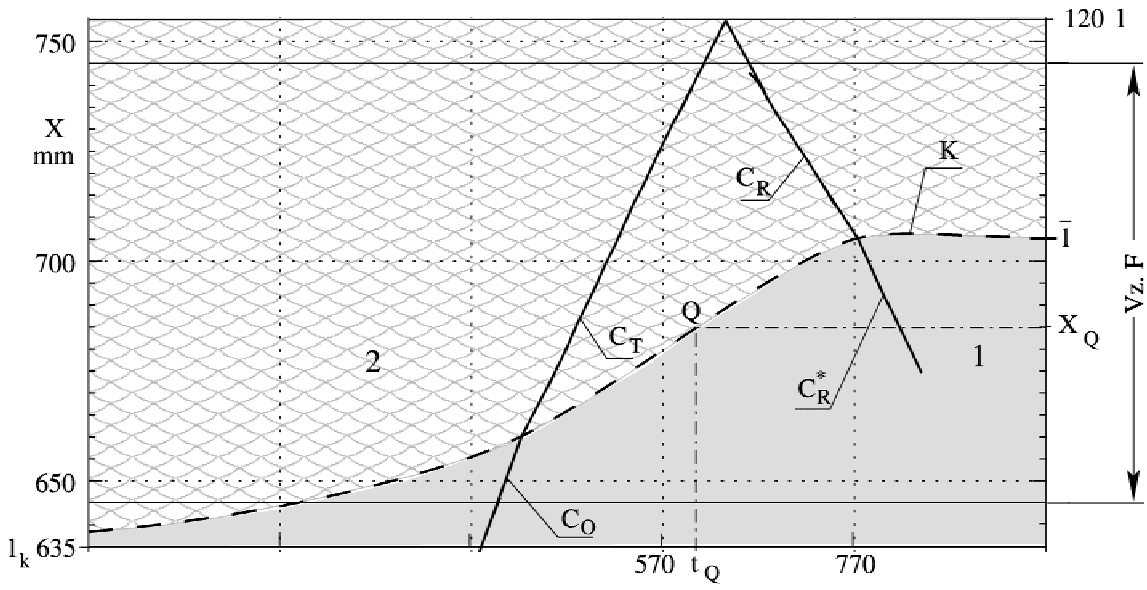

Fig. 6. Wave diagram of interaction between the mixing zone, separating the combustible mixture from argon, with incident and reflected compression waves. C_0, C_T, C_R: incident, refracted, and reflected compression waves. Position of curves C_0, C_T and C_R is defined from a condition $(\partial^2\rho/\partial t^2) = 0$. Curve K corresponds to the motion calculated based on one-dimensional simulation. Within the limits of the measurement error the calculated and measured positions K coincide. Vz. F: visualization area.

the initial mixing zone at a distance of 2 cm from the upper boundary of K. The lower boundary is set at a distance of 12 cm from the upper one.

The quantities for density $\rho(t)$, pressure $p(t)$, temperature $T(t)$ and velocity $u(t)$ found from the one-dimensional numerical simulation are given on the upper boundary (see Sec. 5).

7. RESULTS OF EXPERIMENTS AND NUMERICAL CALCULATIONS: DISCUSSION

7.1. Trajectory of the mixing zone motion

The wave diagram of the process (Fig. 6) is represented by the trajectories of the mixing zone and the incident, transmitted, and reflected compression waves.

The complete numerical simulation of the mixing zone trajectory shows that if calculated and experimental points of the mixing zone trajectory coincide at the beginning stage of motion $t < t_Q$, one can also observe such a coincidence at the final stage $t > t_Q$.

Trajectories of an incident, refracted, and reflected compression wave are presented in the wave diagram by points C_0, C_T, and C_R. The second derivative in these points $\partial^2\rho/\partial x^2$ is equal to zero.

7.2. Excitation and development of the RTI

The evolution of the initial perturbation that has an amplitude $a_i(0) = a_0 < 0.5\,\lambda_i$, can be approximated by the relation

$$a_i(x) = a_i(0)\exp\{W\cdot(2x)^{1/2}\}. \qquad (10)$$

Here $a_i(0)$ is the amplitude of the ith perturbation of the initial mixing zone, x is the travel distance of the mixing zone, counted from its initial position $W = (\mathrm{At}^\circ k)^{1/2}$, where At° is the Atwood number.

Table 1 contains experimental data W for different Atwood numbers. The table also contains values of wavelength λ of the perturbations and thickness δ of layers at which these perturbations are formed. The table also presents the perturbation amplitude growth rate $W(T)$ calculated from the Taylor relation (Taylor, 1950), and $W(D)$, the rate obtained with the method proposed by Duff *et al.* (1962) for a mixing zone of a finite thickness. The quantities $W(T)$ describe the evolution of the linear stage of instability in incompressible media with a discontinuous change of density ($\delta = 0$). The quantities $W(D)$ are also obtained for incompressible media, but the initial mixing zone has a finite thickness δ. Unlike $W(T)$ and $W(D)$, the experimental values W were obtained under the conditions when the RTI development occurs during the simultaneous compression of the mixing zone by waves C_T or C_R. As seen from the table, values W are much less then $W(T)$ and $W(D)$. The

Table 1. *The data of the linear stage of RTI*

Gas	At°	λ mm	$\delta_{in.}$ mm	$W(T)$ $\mathrm{mm}^{-1/2}$	$W(D)$ $\mathrm{mm}^{-1/2}$	W $\mathrm{mm}^{-1/2}$
He	0.64	15	6.2	0.517	0.311	0.166
Ar	0.37	10.7	4.8	0.462	0.270	0.215
Kr	0.64	11.5	1.82	0.591	0.46	0.42
Xe	0.75	11.4	9.0	0.643	0.313	0.519
H_2	0.80	15	4.0	0.579	0.424	0.280

https://doi.org/10.1017/S0263034603213173 Published online by Cambridge University Press

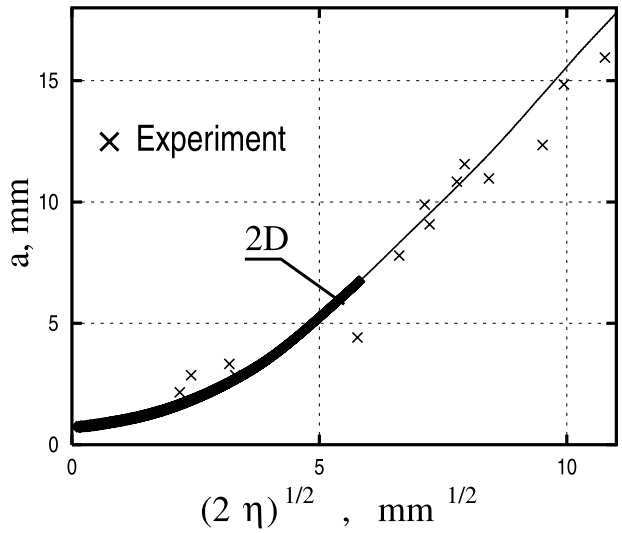

Fig. 7. Comparison of experimental results and calculated ones based on two-dimensional simulation. Thicker part of the solid line: linear stage of the RTI, approximation $a_1 = a_0 \exp(0.4\sqrt{2\eta})$.

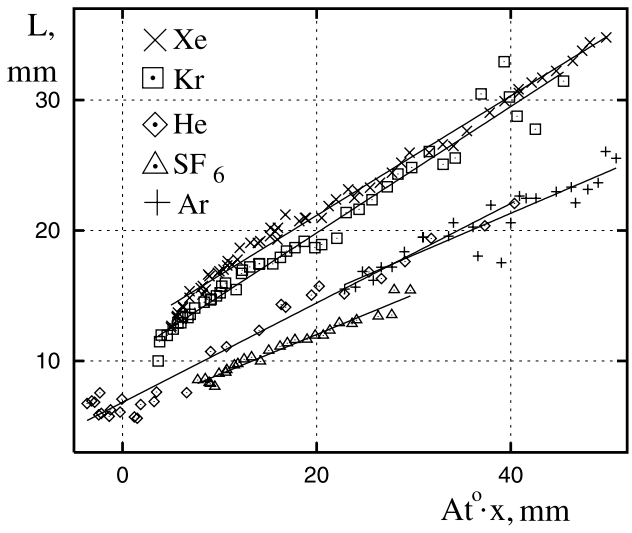

Fig. 9. The penetration depth of gases, $L(x)$, at nonlinear and transitional stages of the RTI. Values $L(\eta)$ are given for He.

latter indicates the influence of compressibility on the RTI evolution. Figure 7 gives results (a_i) of two-dimensional numerical simulations and experimental data for the mixing zone between the combustible mixture and helium at the stage of deceleration. The data are presented in the coordinate system moving with a constant velocity equal to that of the mixing zone at the moment of change of acceleration sign. The principal scheme of definition of traveled distance η in this case is given in Figure 8.

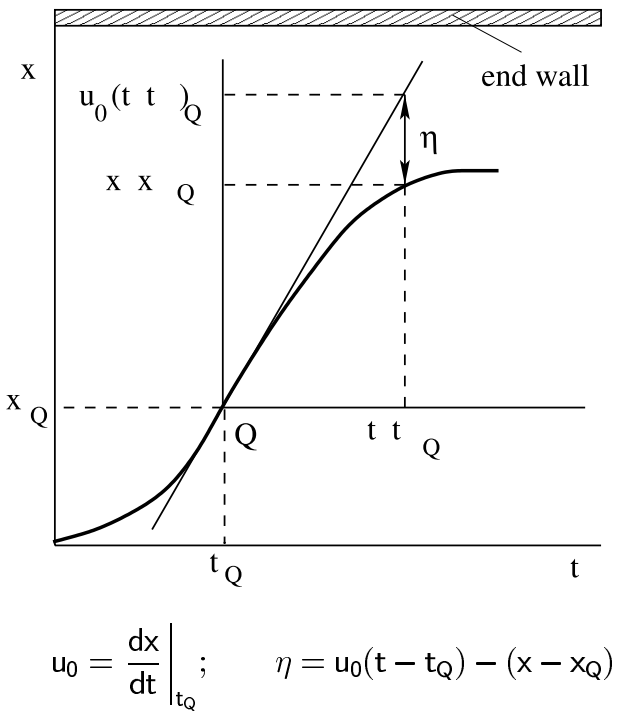

Fig. 8. The principal scheme of definition η.

At $a_i \simeq 0.5\,\lambda_i$, one can observe the beginning and subsequent growth of characteristic distortion of the perturbation form of the surfaces separating the mixing zone from the "pure" gases. The heavy gas penetrates into the light one in the form of narrowing "jets." The light gas penetrates into the heavy one as widening "bubbles"—the nonlinear stage of the RTI. Interferograms of the RTI evolution presented in Figure 2 clearly show this phenomenon. Beginning from this phase, the penetration depth L of one gas into the other, as measured in the experiment, is satisfactorily approximated by a relation

$$L = \alpha_0 \mathrm{At}^\circ (x - x^*) + L_0. \tag{11}$$

Here x^* is the distance traveled by K at the moment of the beginning of the nonlinear stage ($a_i \sim \lambda_i$), At° is the Atwood number, L_0 is a penetration depth of one gas into the other at the moment of transition to the nonlinear stage, and x is the distance traveled by K counted from its initial position.

In Figure 9, the values of L, measured for mixing zones between the combustible mixture and Ar, Kr, Xe, SF_6, and He are given. In Table 2, the values of α_0 are given.

Let us emphasize the combination with helium. Here the instability develops at the stage of the mixing zone deceleration. To calculate α_0 correctly, one needs to take into ac-

Table 2. *Values* $\alpha_0 = dL/[d(At^\circ \cdot x)]$ *and* $\alpha_2 = dL/[d(At^\circ \cdot \eta)]$

Gas	Ar	Kr	Xe	SF_6	He
At°	0.37	0.64	0.75	0.77	0.64
$\alpha_0 \pm 0.11$	0.33	0.38	0.40	0.30	0.38
$\alpha_0 \pm 0.16$	0.34	0.22	0.29		

https://doi.org/10.1017/S0263034603213173 Published online by Cambridge University Press

count only the part of the distance that the mixing zone traveled after the change of acceleration sign. To do this, we have to switch into a coordinate system moving with the constant velocity equal to velocity at the moment $t = t_0$ (see Fig. 8). Then

$$L = \alpha_0 \mathrm{At}^\circ(\eta - \eta^*) + L_0. \tag{12}$$

Here zero points of the coordinate system and time coincide with a point of change of acceleration sign, that is, with the moment when the perturbation growth starts. η^* is the mixing zone position and L_0 is the penetration depth of one gas into the other in the moment of transition to the nonlinear stage of the instability evolution.

7.3. Measurement of mass involved in mixing

Data presented in Table 2 show the growth rate of penetration depth of gases of different densities (the growth rate of distance between the most distant points placed on the different boundaries of the mixing zone). In the case of incompressible media, the growth rate of penetration depth coincides with the growth rate of mass involved in mixing. In conditions of the given experiment, the parameters of media separating the mixing zone from "pure" gases are changing continuously during the motion, so we had to make a direct measurement of the mass of gas involved in mixing. To do this, a method for the definition of the forms of the surfaces separating the mixing zone from the "pure" gases A and B was prepared, on a given level of density change. When defining a volume of the mixing zone in the given moment of time $t = t_i$, the boundaries were set by two tabulated point sets $x_j(y)$, $y_{\min} \le y \le y_{\max}$, $j = 1, 2$. $j = 1$ corresponds to the upper boundary K_b separating the mixing zone from the combustible mixture. $j = 2$ corresponds to the lower boundary K_a separating the mixing zone from gas A. The mixing zone volume is defined as

$$V = H \cdot \int_{y_{\min}}^{y_{\max}} (x_2 - x_1)\, dy, \tag{13}$$

where H is a distance between lateral walls of the tube ($H =$ 7.2 cm).

The mass of matter involved in mixing is defined by a relation

$$M = V(x) \cdot \bar{\rho}(x),$$

where $\bar{\rho} = 0.5(\rho_a + \rho_b)$, and ρ_a and ρ_b are densities of gases A and B on boundaries separating the mixing zone from the "pure" gases.

The data presented in Figure 10 correspond to the growth of the penetration depth $\bar{L}$, volume $\bar{V}$, and mass $\bar{M}$ of gases of different densities as a function of the traveled distance $\bar{x}$ between the combustible mixture and krypton ($\mathrm{At}^\circ = 0.64$). The data correspond to the nonlinear and subsequent stages of the RT instability evolution. $\bar{L}$, $\bar{V}$, and $\bar{M}$ are penetration depth, volume, and mass of gases divided by their values at

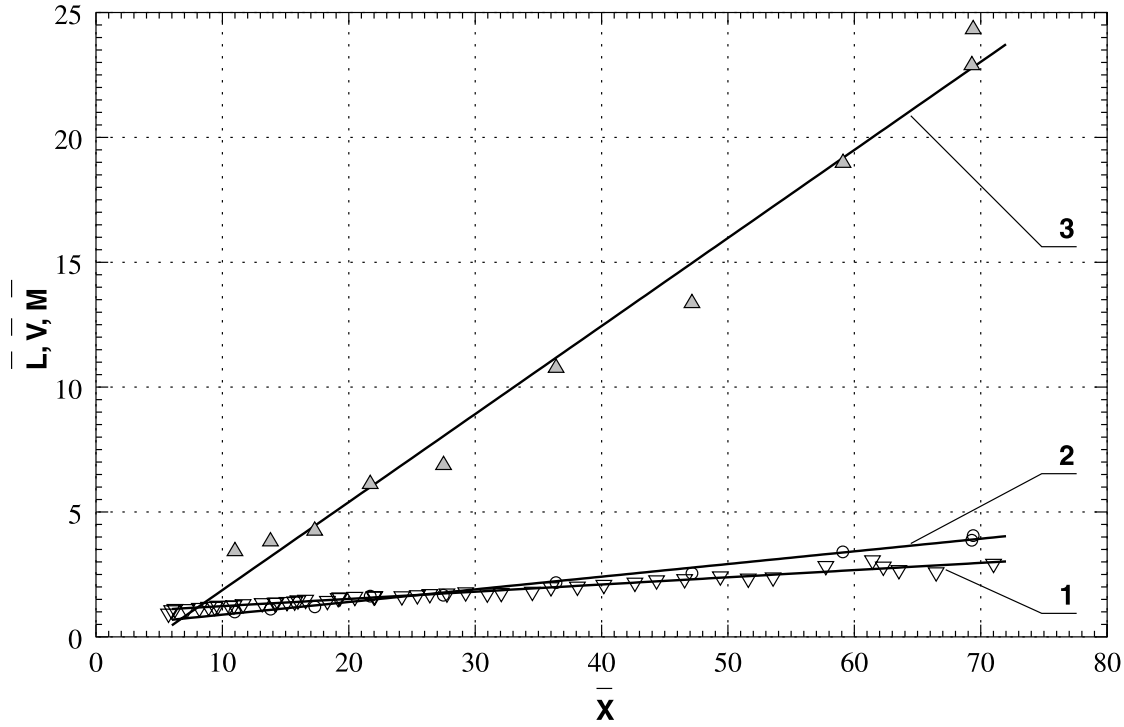

Fig. 10. Values of function $\bar{L}(\bar{x})$, $\bar{V}(\bar{x})$, $\bar{M}(\bar{x})$ for the mixing zone between the combustible mixture and krypton at the stage of accelerated motion.

https://doi.org/10.1017/S0263034603213173 Published online by Cambridge University Press

the moment of transition to the nonlinear stage of the RTI evolution. The traveled distance is nondimensionalized by dividing by L_0, $(x/L_0 = \bar{x})$.

The end plate in the given experiment was placed 230 mm away from the dividing plate. The action of the reflected wave and its "forerunners" within the visualization area did not affect the instability development. It is worth noting that the volume $\bar{V}$ occupied with the mixing zone increases more rapidly as compared to the growth of the penetration depth $\bar{L}$. This may be linked to development of small scale turbulence inside the mixing zone. The growth rate of mass involved in mixing turns out to be an order higher than the rate of the penetration depth because of the density increase caused by compression. Similar results were obtained in experiments with hydrogen ($\mathrm{At}^\circ = 0.8$), where the instability was developed at the stage of interaction with the reflected compression wave.

7.4. Interaction of the mixing zone with reflected compression wave or shock wave

The study of this process has been carried out for the mixing zone between the combustible mixture and argon. The length of the upper part of the channel l_k is 635 mm. The length of the lower part of the channel l–I_k ranged from 100 to 155 mm. In the performed experiments, the density of the driver gas—hydrogen-oxygen mixture—is less than the density of the driven gas—argon. In the stage of accelerated motion of the mixing zone, the RTI was excited. Hence, the penetration depth L of one gas into the other grows. After the beginning of the decelerated motion $(x > x_Q)$ the RTI mechanism is "switched off" and the stratification process begins—separation of gases of different densities, by which L decreases in the sector $x > x_Q$. Such a character of the process is called shockless deceleration.

Figure 11 presents a trajectory of the mixing zone and L values obtained in this experiment. As seen $(x = x_Q)$, the character of function $L(x)$ is changed: Increase is replaced by decrease.

In Table 3 are given the values of the parameters measured in experiments with shockless deceleration. The first column gives the number of the experiment. The second one gives the distance between the channel end plate and the initial position of the mixing zone. In the third and fifth columns, the values of the mixing zone acceleration in the stage of accelerated and decelerated motion are given. In the fourth and sixth columns are the values of dL/dx corresponding to these stages.

To evaluate the suppression of the RTI caused by interaction of the mixing zone with the reflected wave, the following relation was used

$$L = L_0^* - \alpha_2 \mathrm{At}^\circ \eta, \tag{14}$$

where η is calculated using the procedure presented in Figure 8, excluding the fact that the zero point of the coordinate system and time were counted here from the beginning of the decrease of L. Here only the distance traveled by the

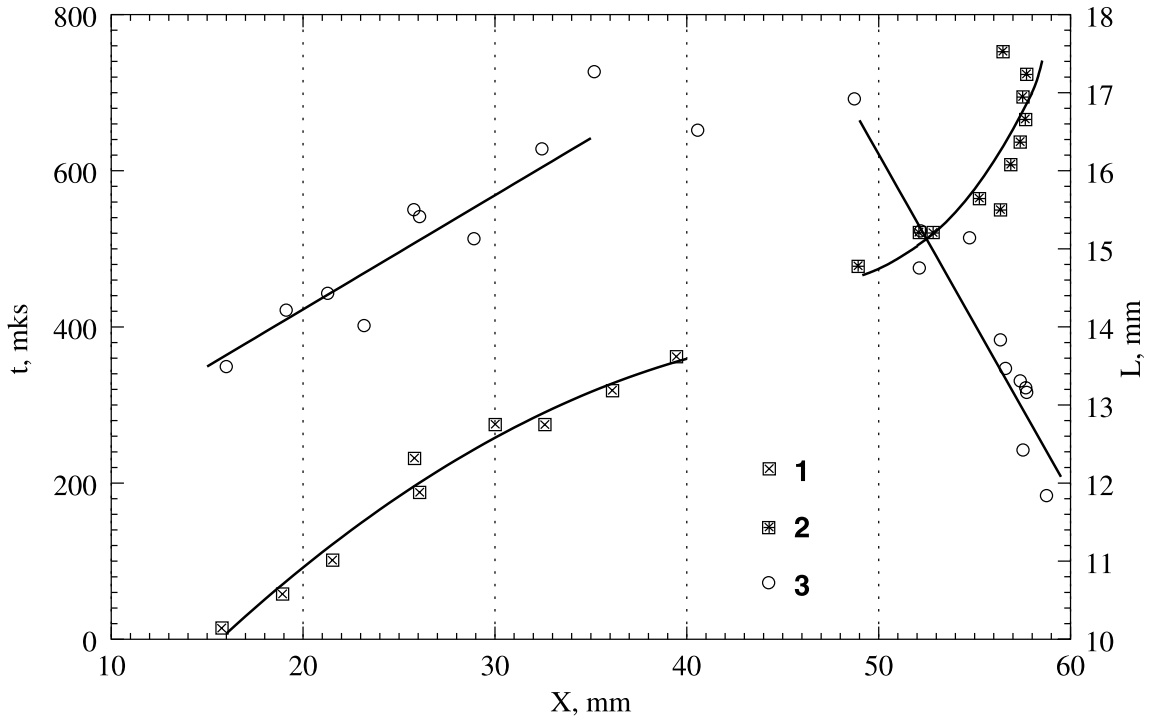

Fig. 11. A trajectory of motion (points 1, 2) and function $L(x)$ (points 3) for the mixing zone between the combustible mixture and argon. Shockless deceleration.

https://doi.org/10.1017/S0263034603213173 Published online by Cambridge University Press

Table 3. *Values of parameters for nonshocked deceleration*

1	2	3	4	5	6
#	$l - l_k$ mm	$g_1 \cdot 10^4$ mm/μs^2	dL_1/dx	$g_2 \cdot 10^4$ mm/μs^2	dL_2/dx
652 A	155	1.18	0.15	−1.34	−0.04
672 A	100	0.913	0.15	−2.38	−0.427
678 A	100	0.717	0.16	−0.513	−0.2
702 A	120	0.955		−4.09	

Table 4. *Values of parameters for shocked deceleration*

1	2	3	4	5	6
#	$l - l_k$ mm	$g_1 \cdot 10^4$ mm/μs^2	dL_1/dx	$g_2 \cdot 10^4$ mm/μs^2	dL_2/dx
650 A	155	1.10	0.104		0.267
653 A	155	0.91	0.128	−7.7	0.196
664 A	155	1.57	0.140	−3.12	0.151
663 A	155	2.43	0.104	−6.5	0.134

mixing zone under action of the negative acceleration was taken into account. The obtained mean value for α_2 is presented in Table 2. The analogous values α_2 were obtained for the combination of the oxygen–hydrogen mixture with krypton or xenon.

An essential change in the evolution of the above-described process is brought by the appearance of a shock wave. The latter is formed in the interval between the end plate and the mixing zone. The collision between this shock wave with the mixing zone leads to the growth of the penetration depth L.

In Figure 12, the diagrams are analogous to ones given in Figure 11, but obtained for a case of shock-induced deceleration are presented.

In all experiments, included in Table 4, the wave fronts that intersect the mixing zone trajectory at $x_Q < x < \bar{l}$ have been distinctly recorded on the interferograms. This interval corresponds to the domain of interaction of the "forerunner" of the reflected compression wave with the mixing zone. The discontinuity of the interferometric bands at the fronts of these waves is roughly 0.5 mm, corresponding to a density change $\Delta\rho \simeq 2.38 \cdot 10^{-5}$ g/cm^3. The velocity of the motion of these waves in the system attached to the mixing zone lies just above the speed of sound (the Mach number equal to 1.05). Such aspect of the function $L(x)$ allows the supposition that the growth of $L(x)$ in the interval $x_0 < x < \bar{l}$ originates from the Richtmyer–Meshkov instability, excited by the interaction of the mixing zone with the shock

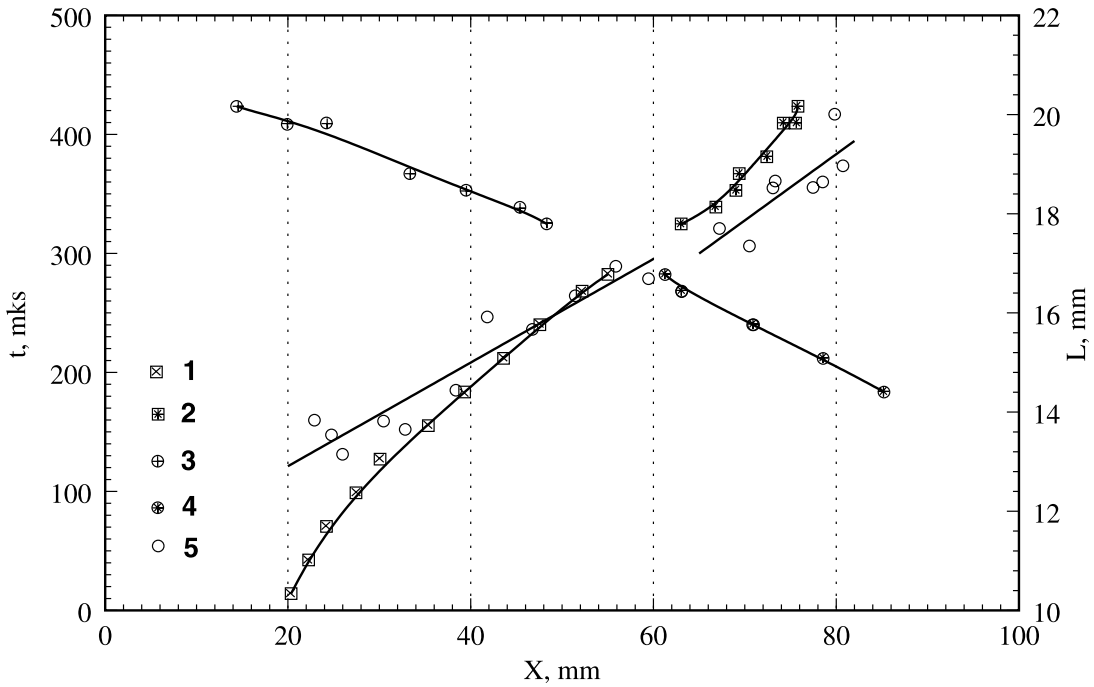

Fig. 12. A trajectory of motion (points 1, 2) and function $L(x)$ (points 5). A trajectory of the reflected shock motion (points 3). A trajectory of the refracted shock motion after interaction with the mixing zone (points 4). Shock-induced deceleration.

https://doi.org/10.1017/S0263034603213173 Published online by Cambridge University Press

waves, which appeared as a result of the evolution of the system of secondary compression waves.

8. CONCLUSION

1. The surfaces that separate the mixing zone from the "pure" gases in the process of the RTI evolution proceed through all the forms well known from the research in incompressible media, which correspond to the linear, nonlinear, and transitional RTI stages.
2. For the linear stage, the growth rate of the amplitude a in compressible media turns out to be significantly less than for incompressible media.
3. For the nonlinear and following phases (transitional, the stage of the ever-growing structures) the penetration depth L of one gas into the other is approximated by a linear dependence on the distance x, traveled by the mixing zone.
4. Inside the mixing zone, a small scale turbulence is excited, which results in increase of the volume $\overline{V}$ growth rate as compared to the penetration depth L growth rate.
5. The braking of the mixing zone, brought by the interaction with the reflected compression wave, is linked to the decrease of the penetration depth L of one gas into the other.
6. In a series of experiments, the braking process, created by the action of the reflected compression wave, is linked to the development of shock waves. At the origin of the development of the latter are secondary compression waves, brought by the interaction of the meniscus-shaped flame front with the channel walls. The mixing zone interaction with the above-mentioned shock waves of low intensity (Mach number near 1.05) leads to the growth of the penetration depth L in the braking process.

REFERENCES

KUCHERENKO, YU.A. *et al.* (1991). *Proc. 3 Int. Workshop on Physics of Compressible Turbulent Mixing*, pp. 427–454.

NIKISHIN, V.V. *et al.* (1994). Preprint # 29, IMM RAS.

SALAMANDRA, G.D. (1974). *Photographic Methods for the Investigation of Fast Proceeding Processes*. Moskva: Iz-vo "Nauka".

SCHNEIDER, M.B. *et al*. (1998). Structure in Rayleigh–Taylor mixing, *Phys. Rev. Lett.* **20**,

TAYLOR, G.L. (1950). *Proc. Roy. Soc. Lon. Ser. A.* **201**, 192–196.

YOUNGS, D.L. (1992). In *Advances in Compressible Turbulent Mixing*, Conf. 8810234, pp. 607–626. Livermore, CA: Lawrence Livermore National Laboratory.

ZAYTSEV, S.G. *et al.* (1991). *Isv. Ac. Sc. USSR, Mechanics of Liquids and Gases*, **6**, 15–21. Translation: *Fluid Dynamics* **26**, 806–811.

ZAYTSEV, S.G. *et al.* (1999). *Euromech Colloquium 403, Futuroscope: Turbulence in High Speed Compressible Flows* (Bonnet, J.P. & Barre, S., eds.).

https://doi.org/10.1017/S0263034603213173 Published online by Cambridge University Press